PCCP

Accepted Manuscript

ROYAL SOCIETY OF CHEMISTRY

www.rsc.org/pccp

Journal Name

ARTICLE TYPE

Cite this: DOI: 10.1039/xxxxxxxxxx

An 'all pigment' model of excitation quenching in LHCII†

Jevgenij Chmeliov,[a,b] William P. Bricker,[c] Cynthia Lo,[c] Elodie Jouin,[d] Leonas Valkunas,[a,b] Alexander V. Ruban,[d] and Christopher D. P. Duffy[d,*]

Received Date
Accepted Date

DOI: 10.1039/xxxxxxxxxx

www.rsc.org/journalname

The rapid, photoprotective down-regulation of plant light-harvesting in high light proceeds via the non-photochemical quenching of chlorophyll excitation energy in the major photosystem II light-harvesting complex LHCII. However, there is currently no consensus regarding the precise mechanism by which excess energy is quenched. Current X-ray structures of this complex correspond to a dissipative conformation and therefore correct microscopic theoretical modelling should capture this property. Despite their accuracy in explaining the steady state spectroscopy of this complex, *chlorophyll-only* models (those that neglect the energetic role of the carotenoids) do not explain the observed fluorescence quenching. To address this gap, we have used a combination of the semi-empirical MNDO-CAS-CI and the Transition Density Cube methods to model all chlorophyll–carotenoid energy transfer pathways in the highly-quenched LHCII X-ray structure. Our simulations reveal that the inclusion of the carotenoids in this microscopic model results in profound excitation quenching, reducing the predicted excitation lifetime of the complex from 4 ns (*chlorophyll-only*) to 67 ps. The model indicates that energy dissipation proceeds via slow excitation transfer (> 20 ps) from chlorophyll to the forbidden S_1 excited state of the centrally-bound lutein molecules followed by the rapid (~ 10 ps) radiationless decay to the ground state, with the latter being assumed from experimental measurements of carotenoid excited state lifetimes. Violaxanthin and neoxanthin do not contribute to this quenching. This work presents the first *all-pigment* microscopic model of LHCII and the first attempt to capture the dissipative character of the known structure.

1 Introduction

During billions of years of evolution, the Sun has always remained the main source of energy for all living beings inhabiting the Earth. An absolute majority of this energy is utilized and then stored in a form of the energy of chemical bounds during the process of photosynthesis, probably one of the most important metabolic reactions occurring *in vivo*. Green plants, algae, and cyanobacteria are not only responsible for the primary step of biomass production, but also fill the Earth's atmosphere with oxygen, a byproduct of photosynthesis required for the vast majority of the heterotrophic living organisms. The 'molecular oxygen factories' of photosynthesis are distributed over the thylakoid membranes, also containing large ensembles of pigment molecules (chlorophylls (Chls) and carotenoids (Cars)), bound to protein scaffold and responsible for the initial steps of photosynthesis, which are commonly referred as 'light reactions'.[1] These pigment–protein supercomplexes, called photosystem I (PSI) and photosystem II (PSII), operate in series to convert solar radiation into storable chemical energy. The mutual arrangement of the pigments within the so-called light-harvesting antenna of the photosystem, as well as their spectroscopic properties, ensures an optimal absorption of the incoming photons and extremely efficient (up to 99%) transfer of the generated electronic excitations towards the reaction center (RC), where these excitations initiate the process of charge separation.[1,2] Despite extensive research taken over the last few decades (see Refs.[3–8] for recent reviews), the specific underlying molecular mechanisms responsible for such an efficient excitation energy transfer within the light-harvesting antenna are still not fully understood.

While such an outstanding quantum efficiency of light harvesting helps photosynthetic organisms to survive and to successfully function at very low levels of illumination, like in aquatic en-

[a] Department of Theoretical Physics, Faculty of Physics, Vilnius University, Saulėtekio Ave. 9, LT-10222 Vilnius, Lithuania.
[b] Institute of Physics, Center for Physical Sciences and Technology, Goštauto 11, LT-01108 Vilnius, Lithuania.
[c] Department of Energy, Environmental and Chemical Engineering, Washington University in St. Louis, 1 Brookings Drive, Saint Louis, MO 63130-4899, USA.
[d] The School of Biological and Chemical Sciences, Queen Mary, University of London, Mile End Road, London E1 4NS, U.K.; E-mail: c.duffy@qmul.ac.uk.
† Electronic Supplementary Information (ESI) available: Inter-pigment excitation transfer times. See DOI: 10.1039/b000000x/

vironment or in deep continual shade, under bright sunlight it has a negative impact and can lead to the photodamage. Indeed, although being rather fast, the turnover rate of the RCs is still finite. As a result, intense illumination saturates its operation and leads to the over-excitation of the light-harvesting antenna thus threatening the formation of free radicals and singlet oxygen capable to 'burn out' the whole photosystem. However, over long ages of evolution, photosynthetic organisms, particularly higher plants, have developed various self-regulatory mechanisms that help them to deal with the excess excitation energy even at the molecular level and, when needed, safely dissipate it as heat.[9] Firstly, the RC itself is capable of adapting to varying external illumination by efficiently regulating the process of charge separation.[10,11] Additionally, other reversible regulatory processes take place in the light-harvesting antenna and make up part of the observed non-photochemical quenching (NPQ) of PSII Chl *a* fluorescence. On a macroscopic thylakoid-level, the most slowly appearing and relaxing form of NPQ, qI, is attributed to actual photoinhibitory damage of a fraction of the RCs in PSII, can take several hours to reverse and is seriously detrimental to the viability of the organism. On a timescale of tens of minutes, the flow of excitation energy towards the RC can be controlled by the reorganization of the antenna complexes thus adjusting the absorption cross-section of the RCs.[12–14] The major part of NPQ—so-called energy-dependent quenching, qE,—is triggered by ΔpH across the thylakoid membrane, increasing during bright sunlight.[9] This most important component of the photoprotective NPQ forms and relaxes within seconds to minutes and operates on a molecular level, though there is still no consensus regarding its underlying molecular mechanism(s).[15–19]

Several possible explanations for the origin of NPQ have been suggested so far, each indirectly supported by some experimental observations.[9] Most of them ascribe the leading role to the carotenoid molecules. The later are indeed indispensable for successful operation of light-harvesting antenna. First of all, they absorb green light, not accessible for chlorophylls, and transfer excitation energy to the latter, thus extending spectral absorption cross-section of photosynthesis. Second, the energy of their triplet state lies below both the triplet state of Chls and singlet state of molecular oxygen, so that Cars can successfully quench dangerous and highly-reactive species and prevent possible photodamage. Finally, it was suggested that their short-living optically-dark first excited state, S_1, can directly participate in the process of NPQ. The discovery of xanthophyll cycle, during which violaxanthin (Vio) is reversibly converted into zeaxanthin (Zea),[20] raised the idea of 'molecular gearshift mechanism'.[21] According to it, the energy of S_1 state of Zea is situated below that of Chls thus allowing the former to act as an excitation energy quencher. Latter, the Zea cation signal was detected in thylakoid membranes under NPQ conditions.[15] As a result, the formation of Zea–Chl charge transfer (CT) state followed by the non-radiative charge recombination was proposed as an origin for NPQ. Meanwhile, other experiments have demonstrated almost instantaneous population of the Car S_1 state upon excitation of Chls[22] as well as Chl fluorescence signal appearing shortly after the two-photon excitation of the Car S_1 state.[23] Both these observations suggest strong interaction between some particular Car and Chl pigments resulting in excitation delocalization over Car–Chl heterodimer, which is also able to operate as an excitation energy trap. Finally, incoherent excitation energy transfer from Chls to Cars, luteins (Lut) in particular, has also been proposed.[17] It is worth noting that an analogue of the last mechanism, this time involving direct energy transfer from a Chl *a* Q_y state to the S_1 state of β-carotene, has recently been shown to be responsible for energy dissipation in the high light-inducible protein (Hlip) HliD in *Synechocystis* sp. PCC 6803.[24]

In order to distinguish between all these possible mechanisms of NPQ, microscopic modeling of excitation energy transfer and quenching in light-harvesting antenna is required. Such theoretical calculations became possible after crystal structure of most photosynthetic pigment–protein complexes—LHCII,[25] CP29[26] and PSII core complexes[27]—had been obtained with a resolution higher than 3 Å, providing essential information on the structural organisation and mutual arrangement of the pigment molecules in these systems. That allowed Novoderezhkin et al. to calculate interaction energies between different Chl pigments in LHCII in dipole–dipole approximation and then to simultaneously fit absorption, linear- and circular-dichroism, and steady-state fluorescence spectra as well as transient absorption kinetics.[28,29] Latter, Müh et al. used highly accurate *ab initio* quantum chemistry methods to calculate Chl–Chl interaction energies, also accounting for the effects of the protein, membrane, and water environment.[30,31] These studies contributed significantly to understanding of inter-chlorophyll excitation energy transfer. However, due to difficulties in the quantum chemistry calculations of the strongly correlated S_1 excited state of the Car pigments, their influence have not yet been studied thoroughly, even though crystal structure of LHCII complexes[25] represents highly quenched species[16] that manifests the presence of some excitation energy traps resembling NPQ *in vivo*.

Recently, we have made a first attempt to explicitly include in our calculations of excitation energy transfer in LHCII trimer one of the carotenoids, namely lutein620 (according to Liu et al.[25] labelling), which is closely associated with the so-called *chlorophyll terminal emitter*, a cluster of three strongly-coupled Chls (namely Chl*a*610–Chl*a*611–Chl*a*612) of the lowest energy.[32] In the present work, we extend this model for the remaining xanthophylls and use the semiempirical MNDO-CAS-CI method to evaluate all the existing inter-pigment couplings and thus to give a reasonable estimate of the quenching ability of various carotenoids.

2 Methods

2.1 Geometry optimisation and calculation of the electronic transitions

The calculation of the resonant inter-pigment couplings in the LHCII trimer follows the procedure outlined in our previous model.[32] This procedure will be briefly summarised here. The starting point is to extract the molecular structure of the 54 pigments (42 Chls and 12 Cars) from the crystal structure of the LHCII trimer as obtained by Liu et al.[25] The next step is to remove the phytol tails from the Chls and to replace them with a

methyl group.[31,32] This vastly reduces the computational expense of the subsequent calculations and has no significant effect on the low-lying excitations originating from the π-conjugated macrocycle. The structures of Chls and Cars were then protonated (since hydrogens are missing from the crystal structure). Finally, it was necessary to optimise the geometry of each pigment (*in vacuo*) in such a way that the bulk structure of each, as defined by the local pigment–protein environment, is preserved.[33] This was achieved via individual density functional theory (DFT) geometry optimisations using the CAM-B3LYP exchange–correlation functional[34] and the 6-31G* Pople basis set,[35] as implemented by the Gaussian 09 quantum chemistry package.[36] To preserve the bulk structure of each pigment molecule, certain dihedral angles were frozen during optimisation: the dihedrals along the conjugated macrocycle for Chls and the ones along the linear conjugated backbone for Cars.[32] These optimised structures were then mapped back onto the LHCII crystal structure in such a way that the average deviation of the heavy atoms was minimised. The resulting largest atomic deviation was smaller than 0.5 Å, *i.e.* much less than the estimated coordinate error of the crystal structure.

As a result of the procedure outlined above, an *in vacuo* matrix of optimised photosynthetic pigments was obtained. The next step in our methodology was a calculation of the low-lying excited states of both Chls and Cars. For Cars, the S_1 and S_2 transitions were computed using the MNDO-CAS-CI method,[37] as implemented by the MOPAC2006 semi-empirical quantum chemistry package.[38] This method has recently been shown to produce a valid description of the low-lying excited states of Cars.[32,39] The active space consisted of 6 π-orbitals (HOMO$-$2, HOMO$-$1, HOMO, LUMO, LUMO+1, and LUMO+2). This method yields a dipole-forbidden ($\mu \simeq 0$D) S_1transition with pseudo A_g^- symmetry and a predominantly double HOMO$\rightarrow$LUMO character as well as a dipole-allowed ($\mu \simeq 20$D) S_2 transition with pseudo B_u^+ symmetry and a predominantly single HOMO$\rightarrow$LUMO character. The validity of these results was discussed extensively in our previous works.[32,39] For consistency, the Chl Q_y transition was calculated using the same 6-π-orbital MNDO-CAS-CI approach that resulted in the dipole-allowed Q_y transitions with the correct single HOMO$\rightarrow$LUMO plus single HOMO$-1\rightarrow$LUMO+1 character.

2.2 Calculation of the inter-pigment couplings

Given that the MNDO-CAS-CI method yields qualitatively reasonable description of the *in vacuo* electronic excitations of both Chls and Cars, we used these results as a basis to calculate the resonant electronic coupling, W, for each pair of pigments. The numerical value of W quantifies the electrostatic interaction between the transition densities of a 'donor' (D) and an 'acceptor' (A) molecule and therefore mediates the corresponding inter-molecular excitation energy transfer. It is composed of two components arising from the Coulomb, J_{DA}, and the exchange, K_{DA}, interactions:

$$W_{\mathrm{DA}} = J_{\mathrm{DA}} - K_{\mathrm{DA}}.$$

The exchange interaction requires significant atomic orbital overlap between the donor and acceptor transition densities and as such falls off exponentially with increasing inter-molecular distance. Therefore it is commonly assumed that the contribution of the exchange interaction to the overall coupling is negligible, $W_{\mathrm{DA}} \approx J_{\mathrm{DA}}$, an assumption we make throughout. In 'traditional' Förster theory, the Coulomb coupling is approximated as an interaction between two point transition dipole moments, μ:[40–42]

$$J_{\mathrm{DA}} \simeq \frac{\kappa_{\mathrm{DA}}}{4\pi\varepsilon\varepsilon_0}\frac{|\mu_{\mathrm{D}}||\mu_{\mathrm{A}}|}{R^3},$$

where R is the centre-of-mass separation of the molecules D and A, κ_{DA} is a dimensionless factor characterising the relative orientation of the two transition dipole moments, and ε is the mean dielectric constant of the protein environment. At the heart of the dipole approximation is the assumption that the inter-molecular distance between donor and acceptor is much greater than the spatial extent of either molecule. This is clearly not a case in a densely-packed pigment–protein complex such as LHCII. Therefore, a more accurate description of the transition density, like the monopole approach[32] or the Transition Density Cube (TDC) method,[43] should be employed. In the current work we utilized the combined MNDO-CAS-CI and TDC approach that has been successfully used to calculate the resonant couplings between Chl *a* and peridinin in the Peridinin–Chlorophyll *a*–Protein (PCP) of dinoflagellates.[44] In this method the true transition densities of the donor and acceptor molecules are approximated as a discrete, three dimensional grid of volume elements (or 'cubes'). The transition density, $M_{\mathrm{D/A}}$, associated with a cube of volume $\delta V = \delta x \cdot \delta y \cdot \delta z$, is given as follows:[44]

$$M_{D/A}(x,y,z) = \int_x^{x+\delta x}\int_y^{y+\delta y}\int_z^{z+\delta z} \Psi_{\mathrm{GS}}\Psi_{\mathrm{EX}}^{*}\,\mathrm{d}x\mathrm{d}y\mathrm{d}z,$$

where Ψ_{GS} and Ψ_{EX} are the ground state and excited state wave functions of the donor/acceptor molecule, respectively. The only approximations involved in a TDC calculation are the predetermined grid size and the accuracy of the quantum mechanical wave functions that the TDCs are constructed from. As the number of grid points are increased, the Coulomb couplings calculated from the donor and acceptor TDCs approach their 'exact' values based on the donor and acceptor wave functions.[43] The number of grid points for the TDCs are chosen based on replicating the value of the exact transition dipole moment from the MNDO-CAS-CI calculation.[44] In these calculations, we use 4 grid points per angstrom, which gives us an average relative error below 0.1 % between the exact MNDO-CAS-CI transition dipole moment and the one being back-calculated from the TDCs. Finally, the inter-pigment Coulomb coupling can be approximated as the sum of all pairwise interactions between the TDCs of the donor and acceptor,

$$J_{\mathrm{DA}} \simeq \sum_{i,j}\frac{e^2}{4\pi\varepsilon\varepsilon_0}\frac{M_{\mathrm{D}}(i)M_{\mathrm{A}}(j)}{\left|\vec{r}_i - \vec{r}_j\right|}, \qquad (1)$$

where the indices i and j label the TDCs of the donor and acceptor molecules and $\vec{r}_i$ denotes the position of a particular volume element.

2.3 Modelling excitation energy transfer and quenching

Quantum chemistry calculations of all the inter-pigment couplings allow us to construct a full excitonic Hamiltonian for LHCII monomer, which in the site basis is expressed as

$$\hat{H} = \sum_{n=1}^{N} E_n |n\rangle \langle n| + \sum_{n \neq m}^{N} J_{nm} |n\rangle \langle m|, \qquad (2)$$

where $N = 18$ is the number of pigments in LHCII monomer (8 Chls *a*, 6 Chls *b*, and 4 Cars), E_n is the energy of the S_1 level of the *n*th pigment, and J_{nm} is the interaction energy between *n*th and *m*th molecules, as defined above in Eq. 1. Assuming the Förster regime of incoherent excitation energy transfer, the inter-pigment transfer rates from the *m*th to the *n*th site, k_{nm}, are given as follows:[29,45]

$$k_{nm} = 2|J_{nm}|^2 \,\mathrm{Re} \int_0^\infty A_n(t) F_m^*(t)\, \mathrm{d}t, \qquad (3)$$

where

$$A_n(t) = \mathrm{e}^{-\mathrm{i}E_n t/\hbar - g_n(t)},$$

$$F_m(t) = \mathrm{e}^{-\mathrm{i}(E_m/\hbar - 2\lambda_m)t - g_m^*(t)}$$

are the Fourier-transfroms of the absorption and fluorescence lineshapes, respectively; $g_n(t)$ is the line-broadening function, and $\hbar\lambda_n$ is the Stokes shift for the corresponding pigment. In terms of the spectral density $C''(\omega)$, the latter two quantities are expressed as

$$g_n(t) = \int_0^\infty \frac{\mathrm{d}\omega}{\pi\omega^2} C_n''(\omega) \left[(1 - \cos(\omega t)) \coth\left(\frac{\hbar\omega}{2k_\mathrm{B}T}\right) + \mathrm{i}(\sin(\omega t) - \omega t) \right],$$

$$\lambda_n = \int_0^\infty \frac{\mathrm{d}\omega}{\pi\omega} C_n''(\omega),$$

where k_B is Boltzmann constant and T denotes the absolute temperature.

The conventional (based on dipole–dipole interactions) Förster theory predicts no excitation energy transfer between Chls and dark (dipole-forbidden) S_1 state of the carotenoids. However, due to relatively small inter-pigment distances in the photosynthetic light-harvesting complexes, energy transfer to the dipole-forbidden states becomes possible.[46,47] In this case the 'absorption spectrum' of the Car S_1 state in Eq. 3 should be treated as a density-of-states (DOS) distribution. Two-photon absorption spectrum of lutein[48] reveals a very broad DOS of the S_1 transition that could be approximately fitted with a Gaussian function with full width at halve maximum (FWHM) of 2880 cm^{-1}. Currently, no empirical spectral density has been determined for the vibronic structure of the Car S_1 state. However, such a broad lineshape can be obtained by postulating the spectral density of the overdamped Brownian oscillator with large reorganization energy λ_0:

$$C_n''(\omega) = 2\lambda_0 \frac{\omega\gamma}{\omega^2 + \gamma^2}, \qquad n \equiv \text{Carotenoid}.$$

Here we fixed the parameter γ, determining the correlation time of the site energy fluctuation, to be equal $\gamma = 53\,\mathrm{cm}^{-1}$ (or $\gamma^{-1} = 100$ fs), a typical value usually used for the light-harvesting pigments. The reorganization energy λ_0 then should be chosen to be of the order of $\lambda_0 = 3400\,\mathrm{cm}^{-1}$ (if static disorder due to inhomogeneous broadening is neglected). We have also tried other parameter pairs ($\gamma^{-1} = 50$ fs, $\lambda_0 = 3180\,\mathrm{cm}^{-1}$ and $\gamma^{-1} = 200$ fs, $\lambda_0 = 3540\,\mathrm{cm}^{-1}$) ensuring approximately the same DOS function of the above-mentioned FWHM. Evidently, in the Förster regime of the excitation energy transfer only the shape of the DOS distribution is important. Therefore, in all three cases of the λ_0 and γ pairs the obtained transfer rates did not differ more than by 1 %. The same spectral density was assumed for other xanthophylls as well. Meanwhile, for the chlorophylls we used spectral density suggested by Renger et al.:

$$C_n''(\omega) = \frac{\pi S_0 \omega^5}{s_1 + s_2} \sum_{i=1}^{2} \frac{s_i}{7!2\omega_i^4} \mathrm{e}^{-\sqrt{\omega/\omega_i}}, \qquad n \equiv \text{Chlorophyll},$$

where $S_0 = 0.5$, $s_1 = 0.8$, $s_2 = 0.5$, $\omega_1 = 0.56\,\mathrm{cm}^{-1}$, and $\omega_2 = 1.94\,\mathrm{cm}^{-1}$.[30,31,49]

Given the inter-pigment excitation hopping rates defined in Eq. 3, the total excitation dynamics in LHCII can be simulated by solving the system of Pauli Master equations

$$\frac{\mathrm{d}}{\mathrm{d}t} P_n(t) = \sum_{m \neq n} [k_{nm} P_m(t) - k_{mn} P_n(t)] - (k_\mathrm{F} + k_\mathrm{NR}) P_n(t), \qquad (4)$$

where $P_n(t)$ is the time-dependent probability for the excitation to reside on the *n*th pigment, k_F is the fluorescence rate, and k_NR is the rate of non-radiative decay. Typical values of $k_\mathrm{F}^{-1} = 16$ ns and $k_\mathrm{NR}^{-1} = 5.3$ ns were chosen for chlorophylls yielding excitation mean lifetime of Chl S_1 state $\tau_\mathrm{Chl} = (k_\mathrm{F} + k_\mathrm{NR})^{-1} \approx 4$ ns. On the other hand, for the dipole-forbidden S_1 state of Cars we have $k_\mathrm{F} = 0$ and very fast non-radiative relaxation of $k_\mathrm{NR}^{-1} \approx 10$ ps. The initial condition of Eq. 4 was chosen to represent a single exciton per LHCII, with equal probabilities to be localised over any of 14 chlorophylls.

The model outlined above can be slightly transformed in order to account for the effect of exciton delocalisation over several pigments. This can be easily done by performing block diagonalisation of the Hamiltonian and thus introducing domains of strongly-coupled molecules (with a coupling greater than some threshold energy, J_cutoff).[29,30,50] A range of various cutoff values (15–120 cm^{-1}) has been used in recent studies on pigment–protein complexes.[29,30,50–53] Obviously, since many inter-pigment electronic couplings are expected to be comparable to the electron–phonon couplings, no single threshold energy resulting in such a simple division of the molecules into domains can be considered precise. In fact, we found that the total calculated excitation decay rate in LHCII was almost insensitive to whether Chl–Chl coherence effects had been accounted for or not. Therefore, in order to be consistent with previous studies,[29,31,32,50] we considered the excitonic delocalisation only between those molecules, for which the calculated incoherent excitation transfer occurred on a sub-ps timescale. Then, assuming instantaneous thermalisation of the excitation within the same domain, the net inter-

Table 1 Inter-pigment couplings in LHCII monomer (in cm^{-1}), obtained in our calculations by using MNDO-CAS-CI approach (lower-left triangle) and those calculated by Müh et al.[30,31] using TD-DFT (upper-right triangle). Diagonal values represent Chl site energies determined by Müh et al.[30]

Pigments	Chl b 601	Chl a 602	Chl a 603	Chl a 604	Chl b 605	Chl b 606	Chl b 607	Chl b 608	Chl b 609	Chl a 610	Chl a 611	Chl a 612	Chl a 613	Chl a 614	Lut 620	Lut 621	Vio 622	Neo 623
Chl b 601	15 405	36.0	-5.0	-3.0	1.0	-2.0	-3.0	3.0	4.0	-5.0	20.0	2.0	-8.0	2.0				
Chl a 602	-35.6	14 940	15.0	6.0	0.0	5.0	6.0	-6.0	-24.0	-5.0	1.0	8.0	-2.0	0.0				
Chl a 603	-5.4	18.1	14 850	-1.0	0.0	-4.0	6.0	4.0	72.0	7.0	-1.0	1.0	1.0	-5.0				
Chl a 604	-1.9	6.3	5.0	14 820	4.0	71.0	24.0	-4.0	-2.0	0.0	-3.0	3.0	2.0	-3.0				
Chl b 605	0.4	-0.5	-0.9	-3.1	15 465	9.0	-4.0	-4.0	0.0	1.0	1.0	-2.0	-1.0	0.0				
Chl b 606	1.6	-5.5	-9.5	77.6	11.3	15 385	16.0	-5.0	2.0	0.0	-2.0	2.0	2.0	-2.0				
Chl b 607	-1.6	5.0	1.0	-17.6	1.1	13.2	15 225	-4.0	-5.0	1.0	-2.0	3.0	3.0	-3.0				
Chl b 608	-1.7	4.8	3.4	-2.5	-3.4	3.0	-3.0	15 215	24.0	43.0	5.0	-1.0	-2.0	1.0				
Chl b 609	-2.4	18.2	62.7	-6.6	-0.2	13.1	-6.3	-14.0	15 475	-2.0	4.0	-1.0	-2.0	2.0				
Chl a 610	-4.1	-10.0	-8.9	4.5	-1.5	-3.4	-0.5	39.8	-1.0	14 790	-26.0	13.0	6.0	-1.0				
Chl a 611	-8.9	-1.8	-1.0	-2.4	1.0	2.3	-1.7	-3.1	-2.5	-29.6	14 950	99.0	-3.0	1.0				
Chl a 612	3.2	11.2	1.9	0.3	2.2	2.9	-1.8	-0.6	-1.2	-12.3	131.4	14 940	0.0	0.0				
Chl a 613	-6.7	-5.5	0.9	-0.3	0.9	1.5	-1.2	-1.4	-1.4	-6.9	-5.6	4.0	14 840	-36.0				
Chl a 614	-3.1	-1.9	-6.8	-3.3	0.4	1.9	-2.5	-1.1	-1.8	-2.0	-3.9	0.7	-60.0	14 940				
Lut 620	0.2	-0.1	0.0	0.5	0.0	-0.3	0.2	0.1	0.2	3.6	1.3	12.2	-2.8	-0.6				
Lut 621	0.3	-2.8	10.8	-5.4	0.2	2.0	-1.9	0.3	0.8	0.4	0.2	-0.6	0.2	0.4	0.0			
Vio 622	1.1	0.0	0.1	0.0	0.0	0.0	0.0	0.0	0.0	0.1	0.4	0.0	3.2	2.4	0.0	0.0		
Neo 623	0.2	-0.4	-0.3	3.9	-0.8	-3.9	0.2	-3.1	0.6	-0.4	0.3	0.9	0.2	0.2	0.0	0.1	0.0	

domain hopping rates are evaluated as follows:[50]

$$k_{\mathrm{dom}\,a\leftarrow\mathrm{dom}\,b} = \sum_{\substack{n\in\mathrm{domain}\,a\\ m\in\mathrm{domain}\,b}} k_{nm}\cdot W_m^{(\mathrm{dom}\,b)},$$

where $W_m^{(\mathrm{dom}\,b)}$ is the Boltzmann factor describing the probability of the corresponding excitonic state within the domain b:

$$W_m^{(\mathrm{dom}\,b)} = \frac{\mathrm{e}^{-E_m/(k_\mathrm{B}T)}}{\sum_{j\in\mathrm{domain}\,b}\mathrm{e}^{-E_j/(k_\mathrm{B}T)}}.$$

This simplified domain model has been recently demonstrated to closely reproduce the full model combining Modified Redfield and Generalised Förster approaches.[50]

3 Results

3.1 Inter-pigment couplings

Inter-chlorophyll couplings, obtained from our quantum-chemistry calculations, are listed in the lower triangle of Table 1. These couplings are very similar to those calculated earlier by Müh et al.,[30,31] see the upper triangle of Table 1 and Fig. 1 for comparison. However, there are some differences in both scale and sign in the low energy region ($J < 10\,\mathrm{cm}^{-1}$). Several factors could lead to such discrepancies. First of all, we naturally expect some differences due to the different quantum chemistry methods used, TD-DFT in study of Müh et al.[30] and MNDO-CAS-CI in our model. Our rational for using the MNDO-CAS-CI method for the Chls was based on treating all photosynthetic pigments within LHCII consistently due to TD-DFT being inappropriate for modelling the low-energy excited states of Cars. Secondly, the transition densities are described very differently in the two studies: Müh et al.[30] fitted transition atomic charges of an analogous

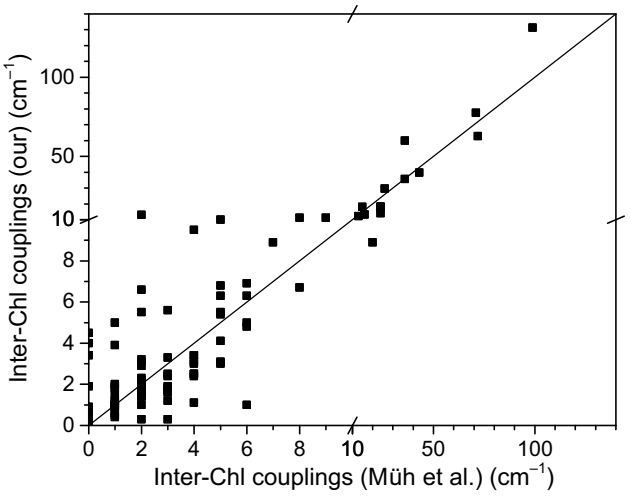

Fig. 1 Comparison of the absolute values of our calculated inter-Chl couplings with those obtained by Müh et al.[30]

electrostatic potential (ESP) associated with the Chl Q_y transition density, while we have adopted the TDC method in which the molecular transition density of each molecule has been discretised into a grid of small, cubic volume elements. The TDC yields an accurate description of the molecular transition density in the regions of space beyond the plane of the Chl molecule rather than the projection of the spatially-extended transition density onto the atomic centres. However, this method is limited by the accuracy of the quantum chemistry method used to obtain the ground and excited state wave functions of Chls and Cars. Importantly, we note that the agreement is much closer for the most significantly coupled Chls. Due to the limitations inherent in using a semi-empirical method we have not explicitly included the di-

electric or electrostatic effect of the protein within our model. However, as in our previous work, the couplings were subject to a rescaling to reflect both inherent discrepencies between the calculated and actual transtion dipole moments of Chls and the solvent effects of the protein environment. The TDCs can be rescaled by a factor of 0.77 to reproduce the vacuum-extrapolated Chl dipole moments reported by Know and Spring.[54] The couplings can then be further rescaled by assumng that the protein envirnoment is a continuous dielectric medium with a relative dielectric constant of $\varepsilon = 2$. This gives an effective scaling factor of 0.38. Since the work of Müh et al.[30] was based on a very careful treatment of the entire LHCII structure, we chose to demonstrate the validity of our method for calculating the inter-molecular couplings generally and then adopted the Chl–Chl couplings obtained by Müh et al.[30] However, for comparison, we have also calculated excitation dynamics arising from our own inter-Chl couplings. Meanwhile, our data for the Chl–Car couplings is novel and therefore it was used throughout. For the site energies of Chls (E_n in Eq. 2) we used those obtained by Müh et al.;[30] site energies for the S_1 transition of Cars, however, are not known. Therefore, we have investigated the effect of possible variations in these energies.

With regard to the Chl–Car couplings, the fact that the S_1 transition has a vanishing dipole moment prevents us from rescaling the TDCs to reproduce some vacuum-extrapolated value. However, we applied the same overall scaling factor (TDCs rescaling plus effect of dielectric screening) of 0.38 used for the Chl–Chl couplings to the Chl–Car ones. We found, in accordance with our previous model,[32] that these were much weaker than the usual Chl–Chl couplings. In good agreement with our previous work, in which we used a less accurate transition monopole approximation of the true Chl and Car transition densities,[32] we find that Lut620 is only appreciably coupled ($J = 12\,\mathrm{cm}^{-1}$) with Chl*a*612 (see Fig. 2). Despite the close cofacial geometry of the Lut620–Chl*a*612, their interaction energy is significantly weaker than that of Chl*a*611–Chl*a*612 ($J = 99\,\mathrm{cm}^{-1}$). We attribute this to the fact the S_1 transition of the Cars is dipole-forbidden. The coupling between Lut620 and more distant neighbouring Chls is significantly weaker ($|J| \sim 3.6$, 1.3, and $2.8\,\mathrm{cm}^{-1}$ for Chl*a*610, Chl*a*611 and Chl*a*613, respectively). Due to the symmetry of the two lutein domains in LHCII[25] we find that Lut621 is similarly only significantly coupled (and even weaker) to Chl*a*603 ($J = 11\,\mathrm{cm}^{-1}$). The Lut621–Chl*a*603 heterodimer possesses the same close, cofacial geometry as its symmetric partner Lut620–Chl*a*612. Similarly it is very weakly coupled to its more distance neighbours. Interestingly, Neo623 and Vio622 do not appear to be significantly coupled to any of their neighbouring Chls. For Neo623, the strongest interactions were found to be with Chl*a*604 and Chl*b*606 ($|J| = 3.9\,\mathrm{cm}^{-1}$), while Vio622 is very weakly coupled to Chl*a*613 and Chl*a*614 ($|J| = 3.2$ and $2.4\,\mathrm{cm}^{-1}$, respectively).

3.2 Excitation energy transfer

Calculations of the incoherent excitation hopping rates between different pigments at room temperature yielded sub-ps timescales for the excitation transfer between Chl*a*610 and Chl*a*611, between Chl*a*611 and Chl*a*612, and between Chl*a*613 and Chl*a*614.

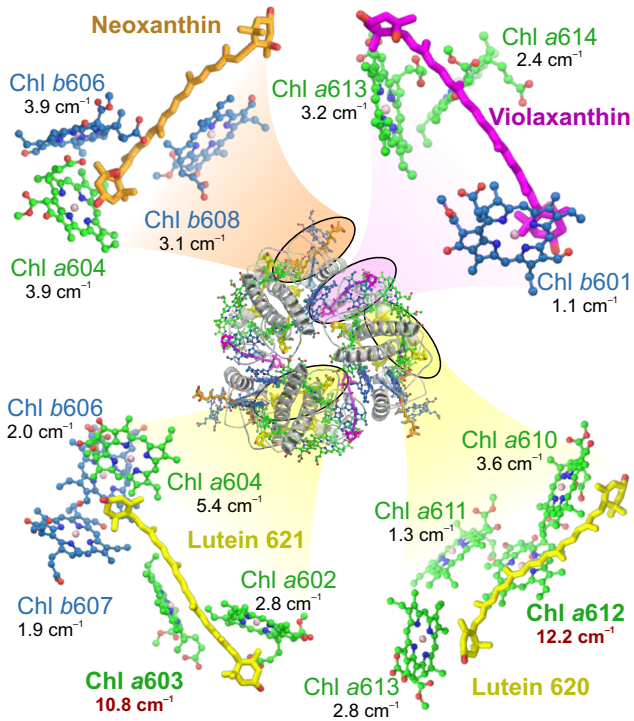

Fig. 2 Crystal structure of the LHCII trimer[25] and the mutual arrangements of the 4 carotenoid molecules and their neighbouring Chls. Numbers represent the coupling strengths between the corresponding Chls and Cars (see also Table 1). Lut620–Chl*a*612 and Lut621–Chl*a*603 pairs exhibit the largest interaction energies.

Therefore the pair Chl*a*613–Chl*a*614 and the triplet Chl*a*610–Chl*a*611–Chl*a*612 were considered to form 2 separate domains with instantaneous equilibration of the excitation within each of them, in consistency with earlier studies of various pigment contribution to the excitonic states.[30,31] After making these adjustments to the model, total excitation dynamics in LHCII monomer was calculated. In the absence of Chl→Car excitation transfer pathway, fluorescence kinetics decays in a single-exponential way with a mean lifetime of 4 ns and fluorescence quantum yield (QY) being $\varphi_F = k_F/(k_F + k_{NR}) = 0.25$. However, inclusion of carotenoids significantly reduces both the fluorescence quantum yield and the mean excitation lifetime. This effect obviously depends on the energy of the S_1 transition of each xanthophyll.

The site energies of Cars are difficult to define as the dipole-forbidden nature of the Car S_1 state prevents its direct experimental measurements. Nevertheless, indirect observations of the S_1 state during the excited-state and transient absorption measurements revealed its energy being about $\sim 13900\,\mathrm{cm}^{-1}$, the same for all four xantophylls bound in LHCIIs.[55] However, both of these methods are likely to probe the relaxed S_1 state rather than the vertical transition, and one would expect the vertical energy to be somewhat higher. In fact, Walla and co-workers directly measured the two-photon absorption spectrum of lutein in solution and found the S_1 peak (the vertical transition) at $\sim 14350\,\mathrm{cm}^{-1}$.[48] Unlike transient and excited-state absorption measurements, this technique probes the vertical transition and therefore represents somewhat more reliable energy of the S_1 state. However, we

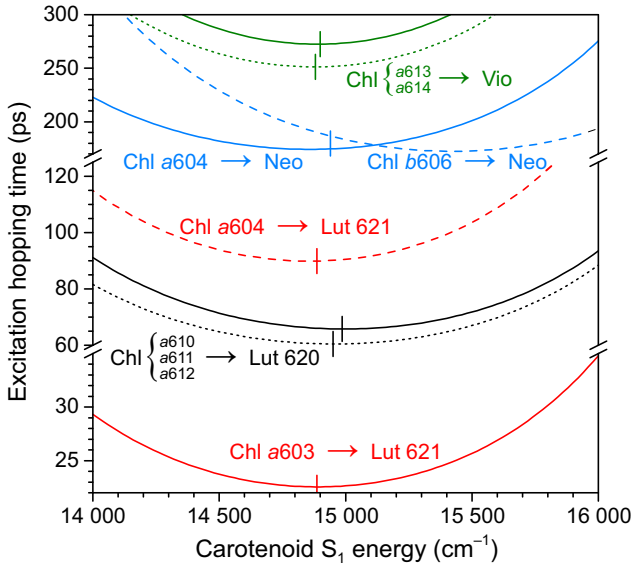

Fig. 3 Chl→Car excitation transfer times *vs* Car S_1 energy level, obtained for different excitation pathways. For Vio and Lut 620, being in close proximity to the domains of strongly-coupled Chls, dotted and solid lines correspond to our-calculated inter-Chl couplings and those obtained by Müh et al.,[30] respectively. Vertical bars indicate energy levels minimizing mean excitation lifetime (see also Table 2).

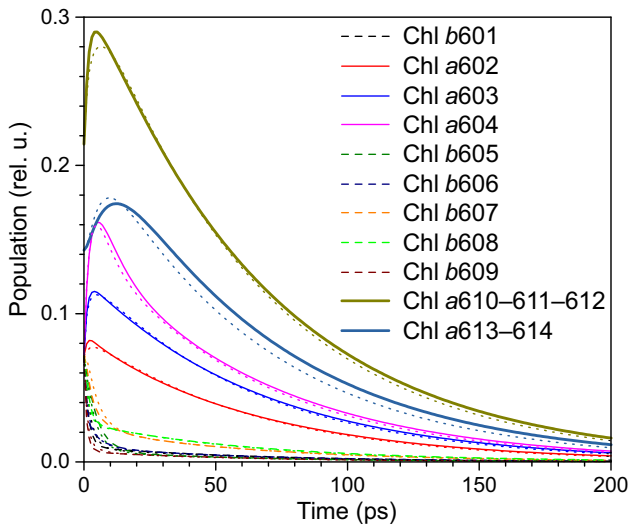

Fig. 4 Populations of different Chl pigments. Solid and dashed lines correspond to Chls *a* and *b*, respectivelly, with inter-Chl couplings calculated by Müh et al.[30] and the Car site energies optimised for the best quenching (see Table 2). For comparison, excitation kinetics calculated from our-obtained inter-Chl couplings are indicated with dotted lines.

naturally expect the local protein/pigment environment inside LHCII to strongly affect the transition energies of all the pigment molecules and, particularly, of Cars.

For this reason we treated the Car site energies as (relatively) free parameters. Initially we chose values that promoted the most efficient total fluorescence quenching, but also explored how the Chl→Car excitation transfer rates depend on Car site energy. This dependence for the most significant Chl-to-Car energy transfer pathways is demonstrated in Fig. 3. We see that the weak Chl–Neo623 and Chl–Vio622 couplings result in very slow energy transfer (about 180 and 270 ps, respectively, see also ESI†). Conversely, Chl→Lut620 and Chl→Lut621 energy transfer times are an order of magnitude faster, a result of their stronger coupling and closer association with their neighbouring Chls. The fastest energy transfer rate, $(23\,\mathrm{ps})^{-1}$, is between Chl*a*603 and Lut621. The calculated rate of incoherent energy transfer from Chl*a*612 to Lut620 was very similar to the one of Chl*a*603→Lut621 pathway; however, exciton delocalisation over the terminal emitter Chl*a*610–Chl*a*611–Chl*a*612 notably reduces the net efficiency of this quenching channel. For the domains of strongly-interacting Chl pigments, our MNDO-CAS-CI calculations resulted in somewhat larger couplings comparing with those obtained by Müh et al.[30] (cf. Table 1). That resulted in slightly faster excitation transfer from these domains to Lut621 and Vio622, as demonstrated with the dotted lines in Fig. 3. Due to the broad nature of the Car S_1 transition all these hopping times are rather insensitive to the variations in energy. For example, the Chl*a*603→Lut621 hopping time varies between ∼23 and ∼30 ps over a wide range of energies between 14000 and 16000 cm^{-1}. However, in all cases we see that there are two dominating channels for Chl→Car energy transfer, both incorporating lutein molecules.

The two Chl→Lut energy transfer pathways result in significant excitation quenching. The strongest possible excitation energy quenching, resulting in mean excitation lifetime of $\tau = 67\,\mathrm{ps}$ (or $\tau = 64\,\mathrm{ps}$ when using our-calculated inter-Chl couplings), was obtained with the S_1 energy levels of xanthophylls indicated with vertical bar in Fig. 3 and listed in Table 2. These energies differ from those determined from the two-photon absorption measurements of the corresponding Cars in solution. This is not surprising, since, as already mentioned, the protein scaffold is known to introduce notable shifts of energy levels of the pigments comparing with their energies *in vacuo* or in solution. In the same Table 2, quantum yields of excitation quenching by the specific Car is also given. In such conditions, the fluorescence QY has dropped about 60 times, from 25 % down to 0.4 %, comparing to the unquenched state. Finally, the contribution of different Chls to the total excitation decay kinetics is shown in Fig. 4. We see very fast (within several ps) excitation transfer from Chl *b* to Chl *a* pigments. After ∼20 ps excitation totally equilibrates over the whole LHCII and then quickly decays with a lifetime of about 70 ps.

Table 2 Energies (in cm^{-1}) of Car S_1 transitions ensuring fastest excitation relaxation in LHCII monomer and the resulting quantum yields (QY) of quenching by particular Car, obtained by using either our values for inter-Chl couplings or those calculated by Müh et al.[30]

Carotenoid	Müh et al. couplings		Our couplings	
	S_1 energy	QY	S_1 energy	QY
Lut 620	14 985	0.36	14 950	0.37
Lut 621	14 890	0.50	14 890	0.49
Vio	14 900	0.06	14 880	0.06
Neo	14 940	0.07	14 930	0.07

4 Discussion

The aim of this study was to produce a microscopic model of the energy transfer dynamics of the LHCII crystal structure that correctly captures the dissipative nature of this configuration. The crystals from which the LHCII structure was obtained exhibit considerable fluorescence quenching relative to the (unknown) *in vivo* light-harvesting conformation, a fluorescence lifetime of ~800 ps in the former as compared to ~4 ns for the latter.[16] This is a feature of the LHCII crystal structure that *chlorophyll-only* models have failed to capture. Our previous work indicated that the inclusion of a single xanthophyll, lutein620, into such a model could explain this fluorescence quenching as originating from direct energy transfer from the chlorophyll terminal emitter domain to lutein620 followed by the intrinsically fast non-radiative decay of the lutein S_1 excited state. For completeness and to test the validity of our previous work, we extended this model to include all pigments present within LHCII.

4.1 Inter-pigment couplings

We used the MNDO-CAS-CI method to compute the Chl and Car S_1 transition densities since this approach, rather than single excitation methods such as TD-DFT or CIS, reproduces the strongly-correlated Car S_1 transition. Using the TDC method we were able to compute the Coulomb interaction between all pigments, both Chl–Chl and, novelly, Chl–Car. These couplings are presented in Table 1. We found that our calculated Chl–Chl couplings were in good agreement with those obtained by Müh et al.,[30] particularly for the strongly-coupled pigments (such as Chl*a*610–Chl*a*611–Chl*a*612). Some inconsistency in both sign and magnitude is apparent for the weakly-interacting molecules which we attribute to the differences in methods of both quantum chemistry and calculation of the electrostatic interactions employed in these two works. The TDC method is known to better represent the transition density in regions out of the plain of the molecule than the transition charge and transition monopole method. However, we note that the Chl–Chl couplings that we calculated in our previous work, based on a transition monopole description of MNDO-CAS-CI excited states, agreed very closely with those calculated via the transition charge method by Müh et al.[30] Moreover, the observed differences in inter-Chl couplings do not notably influence the resulting Chl population dynamics, as demonstrated in Fig. 4 with the dotted lines.

With regard to the Chl–Car couplings, we found that Lut620 is coupled to its close, cofacial neighbour, Chl*a*612, with a strength of $J \approx 12\,\mathrm{cm}^{-1}$. This is in good agreement with $J \approx 14\,\mathrm{cm}^{-1}$ calculated via the transition monopole method in our previous work,[32] indicating that the two methodologies are consistent. Due to the symmetry of the LHCII complex we found that Lut621 was similarly coupled to Chl*a*603 ($J \approx 11\,\mathrm{cm}^{-1}$). The Chl*a*603–Lut621 heterodimer has essentially the same close, cofacial geometry as Chl*a*612–Lut620, albeit with some minor differences in the overall conformation of carotenoid.[56] Interestingly, we found that other two xanthophylls, Vio622 and Neo623, were very weakly coupled to their Chl neighbours. This is supported by earlier experimental studies suggesting that neither violaxanthin nor neoxanthin contribute to light harvesting in LHCII, implying a lack of significant couplings between these pigments and their neighbouring Chls. Indeed, Peterman et al.[57] showed that a xanthophyll with an absorption maximum at 486 nm, attributed to neoxanthin, does not play a significant role in either light-harvesting or triplet quenching in this complex. Later, Bassi and co-workers[58] demonstrated, via spectroscopic analysis, that violaxanthin in LHCII does not transfer excitation energy to neighbouring chlorophylls and therefore also does not participate in light-harvesting. More recently Duffy et al.[59] calculated the Car S_2–Chl Q_x/Soret couplings in LHCII and found that violaxanthin and neoxanthin were significantly less energetically connected to the Chl pool than the two luteins.

One point that we would like to mention at this stage concerns the absolute value of the calculated Chl–Car couplings. The transition dipole moment of the S_1 transition is vanishingly small and therefore prevents accurate empirical rescaling or phase fixing of the raw Car transition densities. As mentioned above, a compromise was to subject the Car transition densities to the rescaling factor (0.38) obtained empirically for the Chls, as outlined in our previous work,[32] but this is an approximation. The calculated Chl–Car couplings are qualitatively reasonable and are consistent with the observed differences between Vio–Chl, Neo–Chl and Lut–Chl couplings. However, they are only strictly meaningful in a relative sense. For the same reason it is not possible to assign a particular phase to the Car transition densities based on the overall phase of a vanishingly small transition dipole moment. However, since the Chl–Car couplings are much weaker than the inter-chlorophyll ones, it is reasonable to assume that energy transfer between the two pigment pools proceeds incoherently. Therefore we assume that any excitonic Chl–Car interactions would be subject to rapid disruption by polaronic effects. As a result, Chl-to-Car energy transfer depends only on the magnitude of the coupling, in accordance to Eq. 3.

4.2 Excitation energy transfer

Within this model the Chl site energies were taken from the work of Müh et al.[30] The site energies of Cars are difficult to define as the dipole-forbidden nature of the Car S_1 state makes direct experimental measurement difficult. Some evaluations of the S_1 energies of the LHCII Cars were made from the excited-state and transient absorption[55] and two-photon absorption[48] measurements. However, we expect the *in vivo* vertical S_1 excitation energies to differ somewhat from those values because the former experiments naturally probe the relaxed S_1 state and the later were performed in solution. We therefore treated the Car S_1 energies as (relatively) free parameters. By optimising these site energies to ensure the fastest possible energy transfer, and therefore the strongest possible excitation quenching (see Table 2) we obtained an excited state lifetime of ~65 ps. Table 2 also shows the relative quenching yields of each Car. Our model implies that quenching proceeds mainly via Chl→Lut energy transfer, while the other Chl–Car channels do not contribute significantly to the overall excitation quenching.

At this point, several things should be noted. First of all, the

overall (the fastest ever possible) quenching predicted by our model exceeds the actual quenching observed in LHCII crystals by an order of magnitude. Indeed, the crystallised LHCIIs had a very broad distribution of fluorescence lifetimes centered at ~800 ps compared to the ~4 ns lifetime of the solubilised (unquenched) trimers.[16] There are several possible sources of this discrepancy. Firstly, due to the absence of rigorous experimental scaling of the Car S_1 transition densities and the lack of a detailed description of the protein/solvent environment it is likely that the calculated Chl–Car couplings represent some over-estimates of the actual physical couplings. Secondly, the Car site energies were chosen to promote the strongest possible quenching rather than to match (relatively poorly defined) *in situ* experimental values. Therefore our model inherently provides a lower limit for excitation lifetime. Longer excitation lifetime may also naturally arise if only one monomer per LHCII trimer is in its quenched state. However, one important conclusion we can draw is that, even given the most favourable site energies and over-estimated couplings, Vio and Neo do not appear to contribute to the excitation quenching. This conclusion confirms an earlier proposal by Ruban et al.[17] that lutein and not violaxanthin or neoxanthin is responsible for fast excess excitation energy dissipation.

Another issue we would like to point out is the fact that, according to our model, both Lut620 and Lut621 contribute similarly to the energy dissipation. This contradicts the original suggestion by Ruban et al.[17] that quenching proceeds via the Chl–Lut620 channel only. However, the structural symmetry of the two lutein domains means that one would expect (as we obtained) very similar coupling profiles for the two molecules. Meanwhile, Yan et al.[56] showed that these two lutein molecules have different conformations within LHCII and therefore might have different functions in the qE mechanism.[56] Due to the fact that the 'dark' nature of the Car S_1 state is largely a product of the well-defined inversion and particle–hole symmetries of the molecule, we would expect non-planar distortions to have a strong effect on the Chl–Car couplings. The differences in geometry were preserved to some extent during our calculations via dihedrally-constrained optimisations, but this procedure itself is not as accurate as obtaining the *real* geometry by optimising the pigments within their protein binding pockets. It is possible that a more 'natural' treatment of these different non-planar distortions may predict some difference. Another possible cause of this symmetry breaking between Lut620 and Lut621 arises from their different locations within the protein. Lut620 is coupled to the Chl terminal emitter of the complex (three Chls of the lowest energy) while Lut621 is coupled to the higher energy Chl*a*602–Chl*a*603–Chl*a*604 domain. It could be expected that Lut620 therefore has greater access to excitation energy due to its proximity to the energy sink and therefore represents the dominant quenching pathway. However, recent studies[28,29,31] have shown that Chl pool in LHCII is rather energetically flat, and our calculations demonstrate that at room temperature excitation equilibrates across the whole complex during the initial ~20 ps. The proposal of Yan et al.[56] therefore looks more likely.

Thirdly, our presented model demonstrates that simple accounting for Car molecules in LHCII crystals does add pathways that can result in strong fluorescence quenching, without the need for more non-trivial mechanisms such as the formation of charge transfer (CT) states[60] or Chl–Car excitonic interactions.[61] However, given that both of these features have been unambiguously observed experimentally, it is not possible (or even correct) to exclude these as playing some role in the quenching mechanism. Additionally, recent single-molecule studies have revealed that LHCII possesses multiple distinct quenching conformations and therefore several quenching pathways may co-exist.[62]

5 Conclusions

We have presented the first *all-pigment* microscopic model of the LHCII trimer that, qualitatively, was able to explain the dissipative character of the known crystal structure and therefore to provide some insight into one of the possible qE mechanisms for *in vivo* LHCII. We found that two centrally-located lutein molecules interact with their closely-associated Chl neighbours in such a way as to yield slow but significant Chl-to-Car energy transfer followed by rapid relaxation of the lutein S_1 state. Additionally, this model tells us little about the conformational switch that forms/relaxes these quenching pathways. The dramatic differences between the Chl–Lut couplings and those of Vio and Neo imply that only modest changes in molecular associations can have a profound impact on the quenching ability of the Cars. We hope that our study will inspire more careful calculations that will take into account the protein/solvent environment as well as its effect on the geometries and couplings within the light-harvesting complex, eventually resulting in deeper understanding of the NPQ mechanisms.

Acknowledgments

This work was partly supported by the Royal Society Wolfson Research Merit Award (A.V.R.). J.C. and L.V. acknowledge the support from the Research Coucil of Lithuania (LMT grant no. MIP-080/2015), and C.D.P.D. thanks the School of Biological and Chemical Sciences, Queen Mary University of London for financial and research support during this project.

References

1 R. E. Blankenship, *Molecular Mechanisms of Photosynthesis*, Blackwell Science, Oxford, 2002, p. 321 p.
2 H. van Amerongen, L. Valkunas and R. van Grondelle, *Photosynthetic Excitons*, World Scientific, Singapore, 2000, p. 590.
3 R. Croce and H. van Amerongen, *J. Photochem. Photobiol. B*, 2011, **104**, 142–153.
4 G. D. Scholes, G. R. Fleming, A. Olaya-Castro and R. van Grondelle, *Nat. Chem.*, 2011, **3**, 763–774.
5 R. Croce and H. van Amerongen, *Photosynth. Res.*, 2013, **116**, 153–166.
6 H. van Amerongen and R. Croce, *Photosynth. Res.*, 2013, **116**, 251–263.
7 C. D. P. Duffy, L. Valkunas and A. V. Ruban, *Phys. Chem. Chem. Phys.*, 2013, **15**, 18752–18770.
8 R. Croce and H. van Amerongen, *Nat. Chem. Biol.*, 2014, **10**, 492–501.

9 A. V. Ruban, M. P. Johnson and C. D. P. Duffy, *Biochim. Biophys. Acta, Bioenerg.*, 2012, **1817**, 167–181.

10 A. O. Goushcha, V. N. Kharkyanen, G. W. Scott and A. R. Holzwarth, *Biophys. J.*, 2000, **79**, 1237–1252.

11 A. O. Goushcha, A. J. Manzo, G. W. Scott, L. N. Christophorov, P. P. Knox, Y. M. Barabash, M. T. Kapoustina, N. M. Berezetska and V. N. Kharkyanen, *Biophys. J.*, 2003, **84**, 1146–1160.

12 E. Wientjes, H. van Amerongen and R. Croce, *J. Phys. Chem. B*, 2013, **117**, 11200–11208.

13 E. Wientjes, H. van Amerongen and R. Croce, *Biochim. Biophys. Acta, Bioenerg.*, 2013, **1827**, 420–426.

14 E. Belgio, E. Kapitonova, J. Chmeliov, C. D. P. Duffy, P. Ungerer, L. Valkunas and A. V. Ruban, *Nat. Commun.*, 2014, **5**, 4433.

15 N. E. Holt, D. Zigmantas, L. Valkunas, X. P. Li, K. K. Niyogi and G. R. Fleming, *Science*, 2005, **307**, 433–436.

16 A. A. Pascal, Z. F. Liu, K. Broess, B. van Oort, H. van Amerongen, C. Wang, P. Horton, B. Robert, W. R. Chang and A. Ruban, *Nature*, 2005, **436**, 134–137.

17 A. V. Ruban, R. Berera, C. Ilioaia, I. H. M. van Stokkum, J. T. M. Kennis, A. A. Pascal, H. van Amerongen, B. Robert, P. Horton and R. van Grondelle, *Nature*, 2007, **450**, 575–578.

18 T. K. Ahn, T. J. Avenson, M. Ballottari, Y. C. Cheng, K. K. Niyogi, R. Bassi and G. R. Fleming, *Science*, 2008, **320**, 794–797.

19 M. G. Müller, P. Lambrev, M. Reus, E. Wientjes, R. Croce and A. R. Holzwarth, *ChemPhysChem*, 2010, **11**, 1289–1296.

20 P. Jahns, D. Latowski and K. Strzalka, *Biochim. Biophys. Acta, Bioenerg.*, 2009, **1787**, 3–14.

21 H. A. Frank, A. Cua, V. Chynwat, A. Young, D. Gosztola and M. R. Wasielewski, *Photosynth. Res.*, 1994, **41**, 389–395.

22 Y.-Z. Ma, N. E. Holt, X.-P. Li, K. K. Niyogi and G. R. Fleming, *Proc. Natl. Acad. Sci. U. S. A.*, 2003, **100**, 4377–4382.

23 S. Bode, C. C. Quentmeier, P.-N. Liao, N. Hafi, T. Barros, L. Wilk, F. Bittner and P. J. Walla, *Proc. Natl. Acad. Sci. U. S. A.*, 2009, **106**, 12311–12316.

24 H. Staleva, J. Komenda, M. K. Shukla, V. Šlouf, R. Kaňa, T. Polívka and R. Sobotka, *Nat. Chem. Biol.*, 2015.

25 Z. F. Liu, H. C. Yan, K. B. Wang, T. Y. Kuang, J. P. Zhang, L. L. Gui, X. M. An and W. R. Chang, *Nature*, 2004, **428**, 287–292.

26 X. Pan, M. Li, T. Wan, L. Wang, C. Jia, Z. Hou, X. Zhao, J. Zhang and W. Chang, *Nat. Struct. Mol. Biol.*, 2011, **18**, 309–315.

27 Y. Umena, K. Kawakami, J.-R. Shen and N. Kamiya, *Nature*, 2011, **473**, 55–60.

28 V. I. Novoderezhkin, M. A. Palacios, H. van Amerongen and R. van Grondelle, *J. Phys. Chem. B*, 2005, **109**, 10493–10504.

29 V. Novoderezhkin, A. Marin and R. van Grondelle, *Phys. Chem. Chem. Phys.*, 2011, **13**, 17093–17103.

30 F. Müh, M. E.-A. Madjet and T. Renger, *J. Phys. Chem. B*, 2010, **114**, 13517–13535.

31 F. Müh, M. E.-A. Madjet and T. Renger, *Photosynth. Res.*, 2012, **111**, 87–101.

32 C. D. P. Duffy, J. Chmeliov, M. Macernis, J. Sulskus, L. Valkunas and A. V. Ruban, *J. Phys. Chem. B*, 2013, **117**, 10974–10986.

33 A. Dreuw, P. H. P. Harbach, J. M. Mewes and M. Wormit, *Theor. Chem. Acc.*, 2010, **125**, 419–426.

34 T. Yanai, D. P. Tew and N. C. Handy, *Chem. Phys. Lett.*, 2004, **393**, 51–57.

35 P. C. Hariharan and J. A. Pople, *Theoret. Chim. Acta*, 1973, **28**, 213–222.

36 M. J. Frisch, G. W. Trucks, H. B. Schlegel *et al.*, *Gaussian-09 Revision A.01*, Gaussian Inc. Wallingford CT 2009.

37 M. J. S. Dewar and W. Thiel, *J. Am. Chem. Soc.*, 1977, **99**, 4899–4907.

38 J. J. P. Stewart, *MOPAC2006*, 2008.

39 M. Macernis, J. Sulskus, C. D. P. Duffy, A. V. Ruban and L. Valkunas, *J. Phys. Chem. A*, 2012, **116**, 9843–9853.

40 T. Förster, *Ann. Phys.*, 1948, **437**, 55–75.

41 T. Förster, *Discuss. Faraday Soc.*, 1959, **27**, 7–17.

42 M. Şener, J. Strümpfer, J. Hsin, D. Chandler, S. Scheuring, C. N. Hunter and K. Schulten, *ChemPhysChem*, 2011, **12**, 518–531.

43 B. P. Krueger, G. D. Scholes and G. R. Fleming, *J. Phys. Chem. B*, 1998, **102**, 5378–5386.

44 W. P. Bricker and C. S. Lo, *J. Phys. Chem. B*, 2014, **118**, 9141–9154.

45 A. Ishizaki, T. R. Calhoun, G. S. Schlau-Cohen and G. R. Fleming, *Phys. Chem. Chem. Phys.*, 2010, **12**, 7319–7337.

46 L. Valkunas, S. Kudzmauskas and G. Juzeliunas, *Sov. Phys. Coll.*, 1985, **25**, 41–47.

47 G. D. Scholes, X. J. Jordanides and G. R. Fleming, *J. Phys. Chem. B*, 2001, **105**, 1640–1651.

48 P. J. Walla, P. A. Linden, K. Ohta and G. R. Fleming, *J. Phys. Chem. A*, 2002, **106**, 1909–1916.

49 T. Renger and R. Marcus, *J. Chem. Phys.*, 2002, **116**, 9997–10019.

50 D. I. G. Bennett, K. Amarnath and G. R. Fleming, *J. Am. Chem. Soc.*, 2013, **135**, 9164–9173.

51 M. Yang and G. R. Fleming, *J. Chem. Phys.*, 2003, **119**, 5614–5622.

52 G. Raszewski and T. Renger, *J. Am. Chem. Soc.*, 2008, **130**, 4431–4446.

53 F. Müh, T. Renger and A. Zouni, *Plant Physiol. Biochem.*, 2008, **46**, 238–264.

54 R. S. Knox and B. Q. Spring, *Photochem. Photobiol.*, 2003, **77**, 497–501.

55 T. Polívka, J. L. Herek, D. Zigmantas, H. E. Akerlund and V. Sundström, *Proc. Natl. Acad. Sci. U. S. A.*, 1999, **96**, 4914–4917.

56 H. C. Yan, P. F. Zhang, C. Wang, Z. F. Liu and W. R. Chang, *Biochem. Biophys. Res. Commun.*, 2007, **355**, 457–463.

57 E. J. Peterman, C. C. Gradinaru, F. Calkoen, J. C. Borst, R. van Grondelle and H. van Amerongen, *Biochemistry*, 1997, **36**, 12208–12215.

58 S. Caffarri, R. Croce, J. Breton and R. Bassi, *J. Biol. Chem.*,

2001, **276**, 35924–35933.

59 C. D. P. Duffy, L. Valkunas and A. V. Ruban, *J. Phys. Chem. B*, 2013, **117**, 7605–7614.

60 M. Wahadoszamen, R. Berera, A. M. Ara, E. Romero and R. van Grondelle, *Phys. Chem. Chem. Phys.*, 2012, **14**, 759–766.

61 P.-N. Liao, C.-P. Holleboom, L. Wilk, W. Kühlbrandt and P. J. Walla, *J. Phys. Chem. B*, 2010, **114**, 15650–15655.

62 G. S. Schlau-Cohen, H.-Y. Yang, T. P. J. Krüger, P. Xu, M. Gwizdala, R. van Grondelle, R. Croce and W. E. Moerner, *J. Phys. Chem. Lett.*, 2015, **6**, 860–867.

Table of contents entry

This work presents the first *all-pigment* microscopic model of major light-harvesting complex of plant and the first attempt to capture the dissipative character of the known structure.